Particle Sizing and Flow Measurements in an Atomizing Mist Jet Nozzle: A Shadowgraphy Approach

O. F. P. Lyons*, T. Persoons and D. B. Murray
Department of Mechanical Engineering
Trinity College Dublin
Dublin, Ireland

Abstract

Particle sizing and velocity measurements are undertaken in an atomizing water mist jet impinging onto a heated copper plate. This study forms part of an investigation into the heat transfer and flow field obtained from the mist jet. The droplet sizes obtained are compared to manufacturer's data. This analysis is performed for the near field and mid field. Ultimately, the effects of particle sizes and velocities will aid the understanding of the heat transfer mechanisms involved.

Introduction

Heat transfer and fluid mechanics of impinging annular jets

Impinging air jets have long been known to achieve superior heat transfer coefficients, with the variation in their local heat transfer coefficients also lending itself to application in areas of large temperature gradients. Their ability to achieve effective cooling rates has led to the implementation of jet cooling in many situations including the replacement of lubricants in some machining operations. Previous work in the research group investigated their effect on grinding temperatures [1].

It is believed that the implementation of a fine water mist into the air stream has the potential to further increase the heat transfer rates. Indeed, Lee et al. [2] state that at droplet diameters of 30-80μm, a "superbly effective cooling scheme" is present. Convective heat transfer coefficients can increase by up to 10 times, through evaporation of an "ultra-thin" liquid film (50-100μm). The dispersal of water droplets into an air flow can be characterized as either spray cooling or mist jet cooling. A spray is obtained by pressurizing the water in the nozzle in order to atomize it. Mist jets use the air pressure to atomize the water. Mist jets thus allow smaller droplet size [3]. The liquid flow can be controlled with less atomization constraints.

Whether a jet is free-surface or submerged depends on the ambient fluid into which they emerge. A submerged jet emerges into a fluid which is the same as the bulk fluid, whereas a free-surface jet emerges into a different fluid. Thus an air jet emerging into air is classified as a submerged jet, while a water jet into air is a free-surface jet. There exists a problem in classifying a mist jet, since a combination of two fluids are emerging into one. For simplicity, since a mist jet is predominantly an air stream with mist particles entrained, it shall be classified as a submerged jet throughout this paper.

For the flow emanating from a conventional round nozzle geometry, there exist several regions of interest from a flow mechanics point of view; the potential core, free jet, impingement and wall jet zones. Misting nozzles that employ shear driven atomization typically employ annular exit conditions so that gas is co-flowing annularly around a central jet of liquid. Excluding bistability and hysteresis identified at low Reynolds numbers by Travnicek, [4], annular nozzles experience recirculation of the flow at low nozzle exit to plate spacings (H/D ratios), as shown in figure 1. At H/D ratios above 6, Lyons et al., [5] show that the annular jet behaves like a jet of circular exit geometry.

Ko and Chan [6, 7] showed that the annular nozzle behaves rather like a rectangular nozzle wrapped around into an annulus. Taking a section through the centre of the jet as shown in figure 1(b), the jet displays as two separate nozzles, each with their own potential core and entrainment effects. Between the two jets, there exists a recirculation zone, where the jets initially start mixing. As can be seen from figure 1 this area continues until the flow reattaches to the opposite jet. In an annular jet used for atomization, the water droplets are effectively "injected" into the flow within the initial mixing region and are entrained into the flow. Outside the two jets, the flow is in contact only with the ambient fluid, leading to effects similar to simple circular exit nozzles. The ambient air is entrained and there exists an area of slower moving fluid. .

*Corresponding author: lyonso@tcd.ie

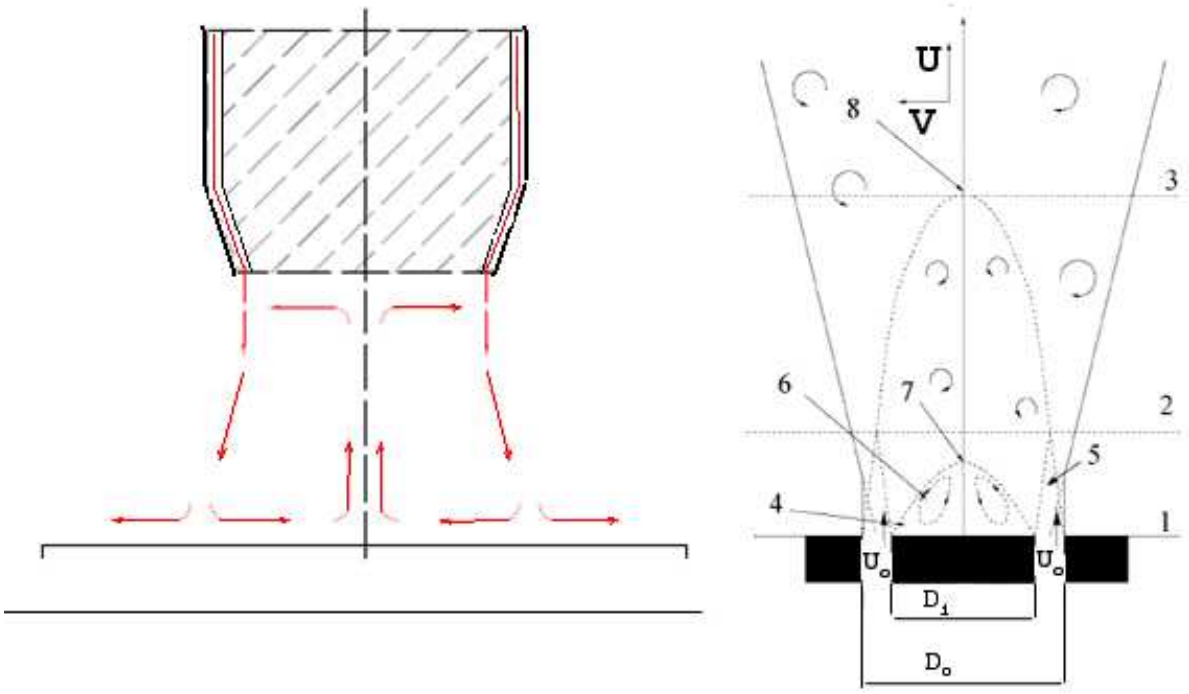

Figure 1. Annular Nozzle: Left: Recirculation of flow at low H/D ratios, [4] Right: Definition of flow structures,[6] : 1, 2, 3, initial, intermediate and fully developed merging zone; 4, recirculation zone; 5, potential core; 6, tore; 7, stagnation point; 8, reattachment point; 9

Liquid atomization in gaseous flows

A spray or mist can be defined as a collection of liquid particles, moving in a controlled fashion along with a gaseous phase. These sprays and mists tend to contain a variety of particle sizes. Several fluid properties affect how a spray is formed, including viscosity, surface tension and density. Surface tension is a representation of the force at the interface between two fluids (for example: liquid water and air) that resists the formation of new surface areas, [8]. Surface tension originates from a difference in cohesion forces between molecules in both materials. Atomization is effectively the break up of a continuous body of fluid into many small bodies of fluid with new surface area. The overall surface area will be thus increased. By breaking up a volume of fluid into smaller bodies with the same combined volume, the overall potential energy increases. This energy is typically supplied by strong shear forces acting on the liquid flow, e.g. by pressure-driven liquid flow through a small orifice, or by entrainment of liquid in a fast-moving gas jet. By stabilizing the fluid, surface tension tends to inhibit the break up of a bulk liquid into smaller droplets, thus for a given flow, fluids with higher surface tension will atomize with a larger average droplet diameter. Viscosity is the resistance of a fluid to being deformed or agitated. Similar to surface tension, high viscosity causes larger average droplet size and prevents the break-up of fluid into smaller droplets. For example, in the case of a liquid jet, fluids with low viscosity will tend to atomize immediately. As the viscosity is increased, the point of atomization moves further away from the nozzle exit, since viscosity will inhibit the growth of any instabilities, delaying the break-up of the liquid, [8]. Density has a similar effect to both surface tension and viscosity and tends to cause larger droplet diameters, by resisting fluid acceleration. Assuming all droplets are spherical, the energy change required to break a parent droplet into n child droplets is:

$$\begin{aligned} \Delta E &= E_{parent} - E_{child} \\ &= \pi d_{parent}^2 \sigma - \pi \sum d_{child}^2 \sigma \end{aligned} \tag{1}$$

Understanding the atomization process is not only of academic importance, but also relevant in combustion, power, medical and manufacturing processes, thus there exists a body of experimental and theoretical work on this phenomenon.

Atomization can also occur when liquid and gas are forced through a small orifice, [9]. This typically requires very high pressure to create atomization, [8]. Since the velocity requires this pressure energy to be converted into

kinetic energy, an increase in velocity needs a corresponding increase in atomization pressure. The velocity will in fact increase with the square of the pressure, [8]. The typical energy cascade is as follows: potential energy stored as pressure in liquid and gas reservoirs is converted into kinetic energy in the nozzle, the breakup of liquid bulk into small droplets with surface tension converts this back into potential energy, some kinetic energy will most likely be dissipated as heat by friction.

In primary atomization, the liquid and gas flows are initially introduced as continuous jets. Close to the nozzle the liquid initially disintegrates into filaments and drops by interacting with the gas stream. Figure 2 shows how the gas and liquid exit a typical annular atomization nozzle. The liquid is injected into an annular co flowing gas stream. The gas is at a high relative velocity, close to the speed of sound in many nozzles. The liquid jet then breaks up due to momentum transfer from the gas to the liquid. Chigier, [10], Engelbert et al, [11], Farago & Chigier, [12], Lashera & Hopfinger, [13] all refer to this as air-blast atomization.

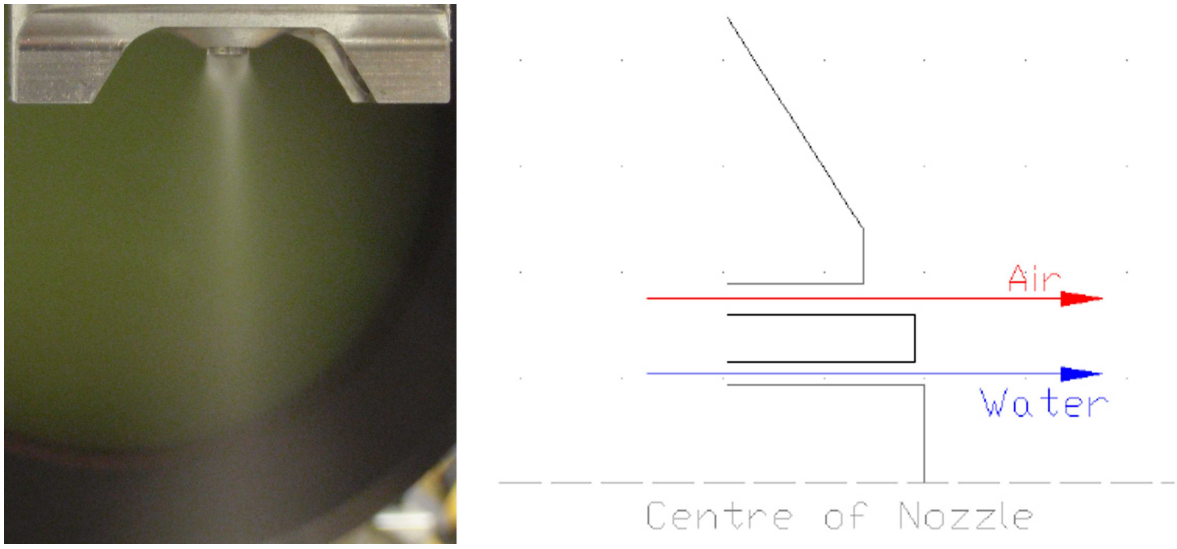

Figure 2. Spray Ppofile of an annular nozzle with co-flowing water and air streams, as shown in the sketch on the right

Shear layer instabilities occurring at the liquid - gas interface effectively cause the liquid to break up, [14], [15]. Upon exiting the nozzle the liquid surface is subject to the Kelvin-Helmholtz instability [9]. The vorticity layer and shear between the air and water layers dictates the most unstable of the Kelvin-Helmholtz instability wavelengths. As this instability develops, it is exposed to the high velocity co-flowing gas. This causes the instabilities to be accelerated, leading to secondary interfacial instabilities, [9], and inducing a Rayleigh-Taylor instability. While this Rayleigh-Taylor instability is causing droplets to be stripped off the liquid layer, the high velocity gas is also accelerating the liquid jet and transmitting momentum to the liquid jet surface, causing large segments to detach, [9].

The overall aim of the research us to characterize the heat transfer from a heated copper plate to an impinging mist jet and to identify the fluid mechanics mechanisms involved. As part of this project, an investigation into the particle sizes and flow of the water droplets provides very interesting information. This paper will predominantly focus on the near field; that is the time averaged droplet distribution in comparison to nozzle manufacturer's data based on inlet air and water pressures. Results will also be reported for the mid field, where the droplet sizes and velocities change as the jet expands away from the nozzle and velocity profiles will be determined. At a later stage this investigation will expand to include data obtained in the far field, close to the impingement plate, which is potentially most interesting from both a flow field and heat transfer perspective.

Materials and Methods

The nozzle used is a Spraying Systems 1/8VAU-SS+SUV152-SS nozzle. The structure of the nozzle provides an inner annular water jet, surrounded by an annular co-flowing jet of air. Variation of either the air or water pressure controls the droplet size. The hydraulic diameter of the air jet is calculated as 0.68mm, with an outer diameter of 3.87mm. The exit area of the water jet is 8.49E-07 m^2 with a hydraulic diameter of 0.28mm. The nozzle is a shear driven atomizing nozzle; that is, the primary mode of atomization is by momentum transfer from

the gas to the liquid flow or shearing of the water jet by the gas stream. The air flow rate is varied from 10 LPM to 40 LPM, this is equivalent to a pressure range from 15 psi (1.03 bar) to 19 psi (1.31), while water flow rate variation is much lower, approx 15 to 22 ml/min and water pressures around 3 psi (0.2 bar). The spray angle is estimated experimentally to be 22°, decreasing to 20° as the air flow rate is increased from 20LPM to 40LPM; the spray angle is not accurately measurable at an air flow rate of 10LPM. These values are quite close to those provided by the manufacturer. The nozzle and the resulting mist spray can be seen in figure 2.

Particle sizing, flow visualization and particle tracking are performed using the shadowgraphy technique. The PIV system contains a Quantronix Darwin-Duo Nd:YLF twin cavity laser (maximum pulse energy of 10 mJ at a repetition rate of 1000 Hz) and a Photron Fastcam SA1 (Lavision HighSpeedStar 6) CMOS camera, (1024 x 1024 pixels, 12 bit). For shadowgraphy, a technique similar to the one used by Berg et al. [16], will be utilized. Thus, pulsed laser light from the PIV system is sent through a diffuser which creates a uniform background illumination. The diffuser contains a diverging lens and a volume of water with dissolved fluorescent dye which is continuously circulating so as to prevent overheating. As the laser beam passes through the diffuser, the Rhodamine-B fluorescent particles in the water-dye solution absorb some of the 527 nm wavelength (green) laser light energy and emit light around 610 nm wavelength (red). This results in a quasi uniform yellowish background illumination. This set-up is shown in figure 3. A 105mm lens and a series of extension tubes (length 150mm) are fitted to the camera in order to increase the magnification factor to 3.33:1 (with a resolution of 6 micron/pixel), mimicking the performance of a long distance microscope, albeit with some loss of light intensity due to the use of a long extension tube.

The mist jet is placed in line with the diffuser and camera. The diffused laser beam creates a uniform background illumination, whereas the water droplets cast a shadow onto the image. Depending on the position of the droplet with respect to the focus plane and depth-of-focus of the camera arrangement, the droplets show up as either sharply focused or blurred images. Out of focus droplets in front of the focus plane (i.e. closer to the camera) appear as rings whereas droplets behind the focus plane (i.e. further away from the camera) appear as blurred spheres. In the particle size algorithm, the appropriate values are set for detection thresholds. To resolve droplet velocity, the camera records images at each laser beam pulse, in a similar manner to 2D PTV. In the analysis conducted in this paper, 500 images are recorded for each test setup and several tests are conducted in order to ensure repeatability.

Using the LaVision Davis 7.2.2 software, the diameter of the water particles can be measured based on the shadow cast by the particle. Additionally the motion of the particles between frames can be detected, allowing particle velocities to be obtained. Both in-plane (x and y) components of the velocities as well as shape and droplet intensity (number of droplets per sample) can be calculated. The shadowgraphy technique provides excellent particle imaging in the range 10μm-100μm. Visualization of particle shape and spray morphology, such as the observation of break-up regions close to the nozzle exit is possible with the shadowgraphy technique, unlike techniques such as Interferometric Mie Imaging and Phase Doppler Interferometry, [16].

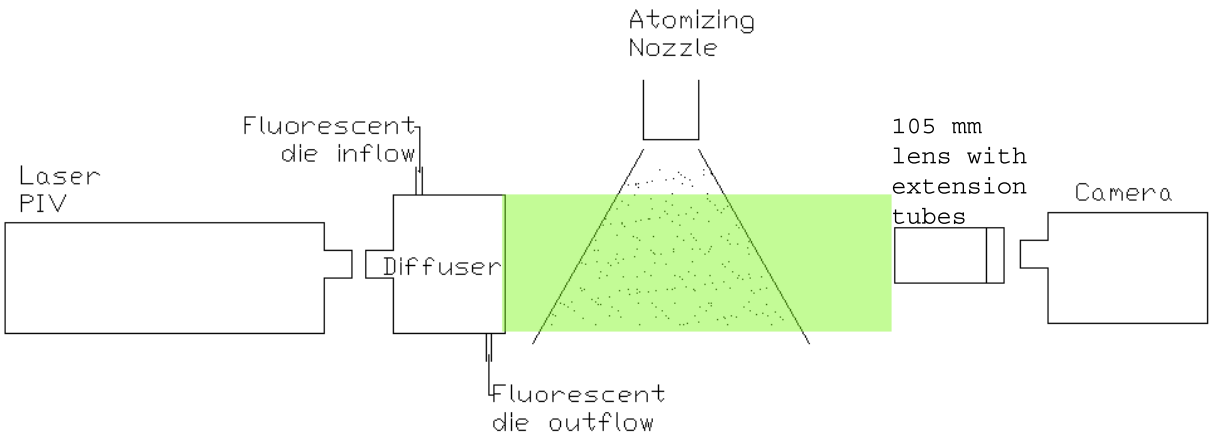

Figure 3. Shadowgraphy setup

There are several issues with the shadowgraphy technique. Due to the small depth of focus, at low air flow rates, where particle number density is low, shadowgraphs can sometimes show no particles. Thus it is necessary

to take a large number of shadowgraphs, in all tests 500 shadowgraphs were recorded, to allow for some images to be devoid of particles. Another artifact of the small depth of focus is that a depth of field calibration is needed to allow measurement of out of focus particles. Detection of particles from the shadowgraphs requires careful analysis and control of the detection parameters. Modifying a value in one direction may result in smaller particles not being detected, while a change in the opposite direction may cause spurious particles due to noise from the camera. Increasing the laser power can result in better data.

Results and Discussion

In this section, a visualization of the spray breakup at nozzle exit through shadowgraphy for a varying air flow rate is presented. Particle sizing and intensity is also undertaken based on a shadowgraphy approach. These results are observed for different air and water flow rates and pressures and their variation with vertical and radial distances from the nozzle exit. Particle diameters are presented as Sauter mean diameters, given in equation 2, where D is the diameter and p_i is the probability of the particle i to be detected, unless otherwise stated.

$$D_{32} = \frac{\sum_{i=1}^{N} \frac{D_i^3}{p_i}}{\sum_{i=1}^{N} \frac{D_i^2}{p_i}} \tag{2}$$

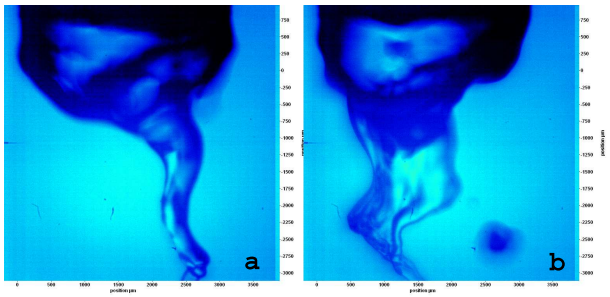

Figure 4. Shadowgraphs at a water flow of 19ml/min and an air flow of 10LPM: a) and b) are taken a different times to show the fluctuating flow from the nozzle

In the first graphs the water flow rate has been kept constant at a flow of 19ml/min. For low flow rates, as in figure 4, the breakup of large filaments tends to oscillate from side to side of the water jet exit. As the air flow rate increases, this effect becomes much less pronounced and the water breaks up in a much more regular pattern. At these low air flow rates, there is insufficient energy to maintain stable atomization; thus the water pressure becomes the controlling factor as to the initial water flow. The air speed cannot strip particles from the flow and the point of atomization is delayed.

The most unstable wavelength of the Kelvin-Helmholtz instability is determined by the incoming vorticity layer, formed in the gas flow. These initial atomization waves are accelerated by the high speed gas stream. As the air velocity is decreased, this momentum transfer from gas to liquid is decreased.

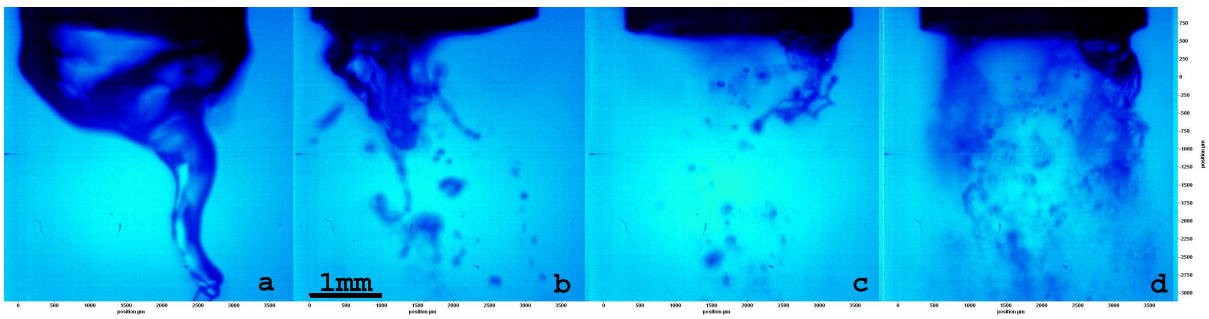

Figure 5. Shadowgraphs at nozzle exit for air flow rates of a)10LPM, b)20LPM, c)30LPM, d)40LPM (each image is 4mm x 4mm

At the lower air flow rates, water jet 'cylinder' maintains its integrity for a longer distance from the nozzle before breaking up . As the air flow rate is increased the initial filaments become shorter and breakup of the filament into droplets happens closer to the nozzle. Thus as the air flow rate is decreased, the point of initial breakup is moved away from the nozzle exit. This effect can be observed in the series of shadowgraphs in figure 5. At the lower flow rates there is less energy available for atomization and thus it takes longer for droplets to be stripped off the water flow; the flow stays as a coherent body of fluid to greater distances from the nozzle exit.

In general, for low air flow rates, experiments becomes less repeatable, since the droplets are not breaking up as quickly and larger droplets are produced. This means that there are a smaller number of larger droplets, some of which appear not to be following the airflow as accurately as the smaller particles.

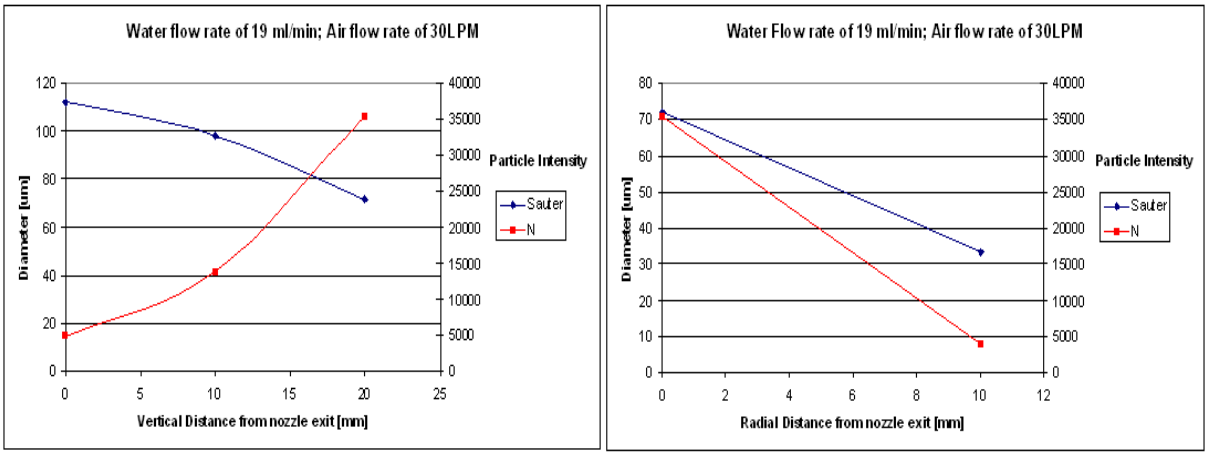

Figure 6. Particle size (Sauter mean diameter) and number density against vertical and radial distance from nozzle exit centre point

As can be seen from figure 6 particle diameters and particle number densities or intensities vary with both vertical distance from the nozzle exit and radial distance from the centre of the nozzle body. Where the vertical distance is varied, the radial location is that of the geometric centre, and where radial distance is varied, this is at a vertical distance of 20mm from the nozzle exit. N is the number of particle recorded and N' is corrected for particles partially obscured by the border. It should be noted that measurements of particle diameter and intensity are based on shadowgraphs recorded at each location; thus 0mm refers to a shadowgraph that was recorded at the nozzle exit. For an air flow of 30 LPM and a water flow rate of 19 ml/min, the particles in the first shadowgraph have a sauter diameter of 112 μm dropping to 98 μm and 72 μm at H=10mm, and H=20mm respectively. The particle intensity ranges from 5,000 to 14,000 to 35,000 for the same values. There are several reasons for this. At the nozzle exit, not all the water filament has been atomized; thus there will be less particles. Additionally, the water has only just been exposed to the gas stream; there has been insufficient time for the momentum of the gas stream to be transferred to the liquid flow and for the interfacial instabilities to build up. With increasing distance from the nozzle, the particles have been exposed to more of the co-flowing gas stream, resulting in the growth of the instabilities and more particles being stripped from the initial filament, which appears to have broken up completely by the time the shadowgraph of H=10mm has been recorded. There is more energy available to break up the droplets further; resulting in a decrease in particle size. Once the initial filament has broken up, one might expect the droplet intensity to decrease with increasing distance from the nozzle, since the particles will be spread out to greater radial distances. Countering this effect is the breakup of droplets into smaller droplets, and thus increasing the droplet intensity. For low to medium exit distances, this should be the predominant driving mechanism behind droplet intensity.

From figure 7 it can be seen that the particle size tends to decrease as the air flow is increased. It is evident from figure 8 that particle sizes increase with increasing water flow rate. This occurs because the process of atomization is shear driven atomization, whereby particles tend to increase with decreasing slip velocity, $u_g - u_f$. The energy needed to break up each large parent droplet into smaller droplets is defined by equation 1. For low air flow rates, the energy available is not sufficient for the larger droplets to be broken into smaller droplets. An obvious consequence of this larger droplet distribution is that for a constant water flow rate, the particle intensity will decrease; this is clearly evident from figure 7. By representing the total droplet volume flux as the droplet

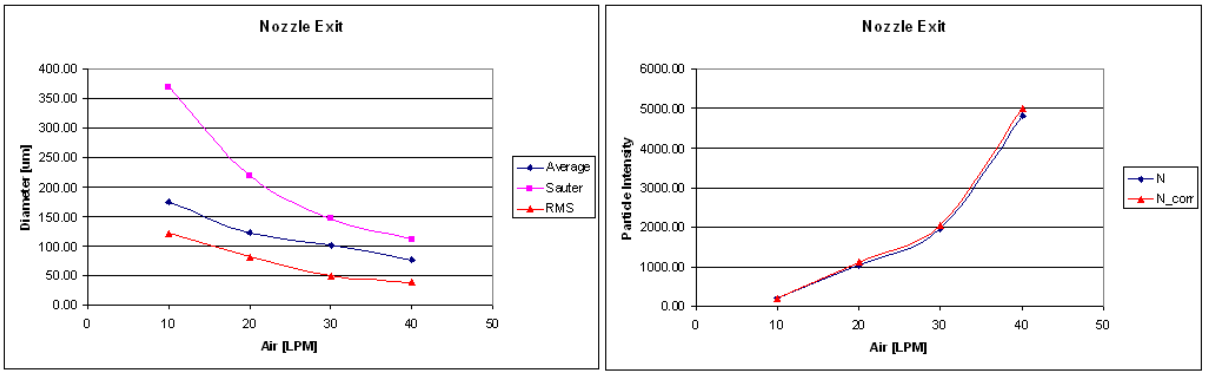

Figure 7. Particle diameter and intensity plotted against air flow rate for constant water flow of 19 ml/min: Sauter, Average and RMS

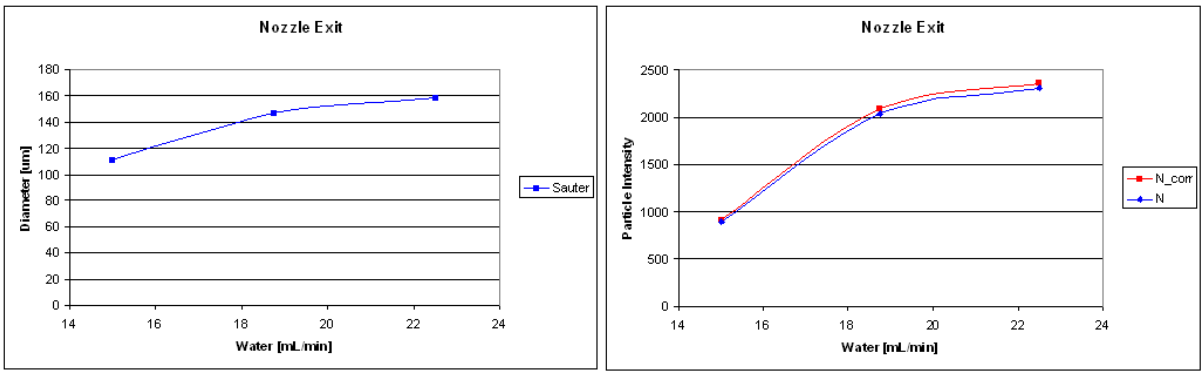

Figure 8. Particle diameter and intensity plotted against water flow rate for constant water flow of 30 LPM

diameter cubed multiplied by the droplet intensity, this can be compared with air flow. Larger droplets break up into smaller droplets and increase the droplet intensity; thus this droplet volume flux should stay fairly constant for constant water flow rate. Table 1 shows a representation of the droplet volume based on the sauter diameter and the number of particles recorded. From table 1, it can be seen that this value stay broadly constant for air flow rates of 20-40 LPM, however the droplet volume decreases by quite a large amount as the air flow rate is decreased to 10 LPM. As is evident from the shadowgraphs in figure 5, the majority of the liquid has not yet been atomized, and is thus exempt from the particle sizing algorithms. For air flow rates of 20-40 LPM a greater proportion of water has been atomized.

At greater radial distances, droplet diameter and intensity both decrease as seen from figure 6. This trend is different to the other trends whereby a decreasing diameter was coupled with an increasing intensity. At a radial distance of 10 mm, the droplets are probably outside the mist spray core, and thus fewer droplets will exist. possibly, in a similar manner to entrainment within an air only flow from a submerged jet, there exists a zone where particles appear to be caught in the ambient air. The smaller particles require less energy to be thrown out of the core and thus it is more probable for smaller particles to appear in this region. Further analysis is required to investigate this effect further; testing is planned at smaller radial distances from the centre and a comparison of this effect at various nozzle exit distances will also be carried out.

The exit velocity of the water is based on the flow rate of water through the nozzle divided by the exit area. The actual exit area of the water jet is difficult to measure accurately, and is undertaken with a microscope. Combining the air and water velocities into the Weber number allows a study of the effect of the shearing of the air-water interface and the resulting droplet distributions.

As the air velocity is decreased the particle distributions become noisier, and have a less normal pattern. Especially at an air flow rate of 10LPM, the particle sizes are not distributed cleanly and there exists several larger particles away from the main distributions. The repeatability of observing these larger particles is not very high, suggesting an unstable nature of the flow. This can be seen from figure 9.

Outside of this mist spray core, where most of the droplets are present, there exists a fine mist flow where a

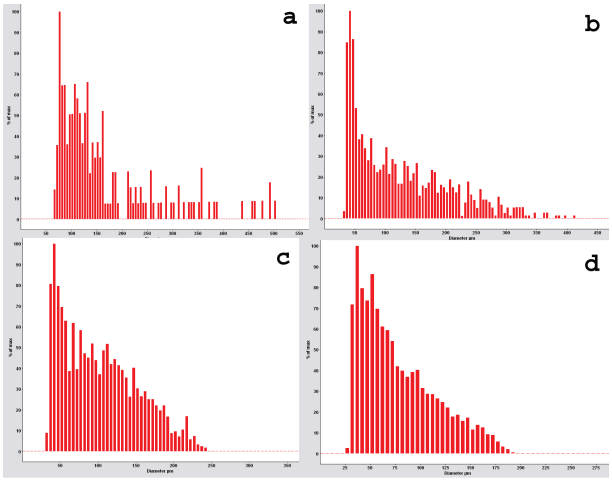

Figure 9. Particle size distributions at nozzle exit for air flow rates: a) 10LPM b) 20LPM c) 30LPMd) 40LPM

Table 1. Representation of droplet volume flux against air flow for constant water flow rate

Air [LPM]	$D^3 * N$ [μm^3]
10	9.78E+08
20	1.92E+09
30	2.00E+09
40	2.09E+09

much smaller concentration of mist exists. The particle sizes are smaller in this region and the velocities lower and less regular (more turbulent); that is they do not appear to follow the air flow velocity in direction nor magnitude. This is possibly due to entrainment effects of the flow.

In a similar manner to that of air only flow, air outside a potential core is entrained into the ambient fluid. Since the mist particles, especially the smaller particles, predominantly follow the air flow, particles outside of this central region where flow velocity is maintained, behave in a much more turbulent manner.

This can be seen from the lower numbers of particles in the outer regions, figure 6. Particles outside the mixing zone tend to have an erratic velocity, not following the flow as much as the other particles. Indeed, some particles appear to be thrown out of the jet flow, and are merely present in the ambient air.

Conclusions

A rig has been constructed which is capable of identifying flow structures in an atomizing nozzle. Droplet diameter and velocity measurements are possible within a small depth of focus, but some particles are not recorded due to being out of focus; particles can also appear larger due to defocussing, but this is usually detectable.

Data shows the droplet formation follows typical shear driven atomization; particle diameters decrease with increasing air and decreasing water flow rates, while particle number density increases with increasing air and decreasing water flow rates.

Particle sizes decrease with increasing vertical and radial distance from the nozzle exit, although due to different underlying reasons. The particle intensity increases with increasing vertical distance from the nozzle while falls with increasing radial distance from the geometric centre.

At low air flow rates, atomization becomes unstable and shadowgraphy results become unrepeatable.

This ultimate aim of this research is to identify the heat transfer and flow mechanisms responsible for cooling of a flat plate by an impinging mist jet. This will involve simultaneous measurements of both droplet dynamics, flow field phenomena and heat transfer characteristics.

Acknowledgments

The authors acknowledge the technical support staff of the Mechanical and Manufacturing Engineering Department of Trinity College.

The authors would like to thank IRCSET for funding provided for this project.

References

[1] Donovan, T. S. O., Murray, D. B., and Torrance, A. A., 2006. "Jet heat transfer in the vicinity of a rotating grinding wheel". *Proc. I.Mech. E. Part C-J. Mech.Eng.Sci*, ***220***(6), pp. 837–845.

[2] Lee, S. L., Yang, Z. H., and Hsyua, Y., 1994. "Cooling of a heated surface by mist flow". *Journal of Heat Transfer,* ***116***(1), pp. 167–172.

[3] Lee, S., Number 8/October 2005. "Heat transfer characteristics during mist cooling on a heated cylinder". *Heat Transfer Engineering,* ***26***, pp. 24–31(8).

[4] Travnicek, Z., and Tesar, V., 2008. "Hysteretic behavior of annular impinging jets". *5th European Thermal-Sciences Conference, The Netherlands, 2008*.

[5] Lyons, O. F. P., Murray, D. B., Byrne, G., and Persoons, T., 2009. "Time averaged and fluctuating heat transfer measurements in an atomising mist jet nozzle". *Proceedings of IMECE2009 2009 ASME International Mechanical Engineering Congress and Exposition, IMECE2009-11244, November 13-19, Lake Buena Vista, Florida, USA,* ***1***(1).

[6] Ko, N. W. M., and Chan, W. T., 1978. "Similarity in the initial region of annular jets: three configurations". *Journal of Fluid Mechanics,* ***84***(4), pp. 641–56.

[7] Chan, W. T., and Ko, N. W. M., 1978. "Coherent structures in the outer mixing region of annular jets". *Journal of Fluid Mechanics,* ***89***(3), pp. 515–533.

[8] Lefebvre, A. H., 1989. *Atomization and sprays*. CRC Press.

[9] Gorokhovski, M., and Herrmann, M., 2008. "Modeling Primary Atomization". *Annual Review of Fluid Mechanics,* ***40***, Jan., pp. 343–366.

[10] Chigier, N., 1991. "The physics of atomization. plenary lecture". *Proceedings of the International Conference on Liquid Atomization and Spray Systems, 5th, ICLASS-91, Gaithersburg*, pp. 49–64.

[11] Engelbert, C., Hardalupas, Y., and Whitelaw, J. H., 1995. "Breakup phenomena in coaxial airblast atomizers". *Proceedings: Mathematical and Physical Sciences,* ***451***(1941), pp. 189–229.

[12] Farago, Z., and Chigier, N., 1992. "Morphological classification of disintegration of round liquid jets in a coaxial air stream". *Atomization Sprays,* ***2***, p. 137.

[13] Lasheras, J. C., and Hopfinger, E. J., 2000. "Liquid Jet Instability and Atomization in a Coaxial Gas Stream". *Annual Review of Fluid Mechanics,* ***32***, pp. 275–308.

[14] Varga, C. M., Lasheras, J. C., and Hopfinger, E. J., 2003. "Initial breakup of a small-diameter liquid jet by a high-speed gas stream". *Journal of Fluid Mechanics,* ***497***, pp. 405–434.

[15] Marmottant, P., and Villermaux, E., 2004. "On spray formation". *Journal of Fluid Mechanics,* ***498***, pp. 73–111.

[16] Berg, T., 2006. "Comparison of particle size and velocity investigations in sprays carried out by means of different measurement techniques". *ICLASS '06, Kyoto, Japan*.